ACS Sustainable Chemistry & Engineering

Research Article

Cite This: ACS Sustainable Chem. Eng. 2019, 7, 12948−12954

pubs.acs.org/journal/ascecg

New Structural Carbons via Industrial Gas Explosion for Hybrid Cathodes in Li−S Batteries

Xiaohua Feng,*,† Xuanning Huang,‡ Yangzhou Ma,*,‡ Guangsheng Song,‡ and Hua Li*,†

†Key Laboratory of Marine Materials and Related Technologies, Zhejiang Key Laboratory of Marine Materials and Protective Technologies, Ningbo Institute of Materials Technology and Engineering, Chinese Academy of Sciences, Ningbo 315201, China

‡School of Materials Science and Engineering, Anhui University of Technology, Maanshan, Anhui 243002, China

Supporting Information

ABSTRACT: Hereinafter, we report onion-like carbon (OLC) and fullerene-like carbon (FLC) materials synthesized via 2,4,6-trinitrotoluene (TNT) and 1,3,5-trinitro-1,3,5-triazine (Royal Demolition Explosive, RDX) detonation technique and acetylene gas explosion process, respectively. Abundant micropores, mesopores, and different spatial structures exist inside the two carbon materials. They demonstrate good conductivity and sulfur storage capacity, and various rich pore structures, inhibiting the shuttle effect of the solved lithium polysulfide in the charge−discharge process. The pore size distribution, pore volume, specific surface area, electronic conductivity, composite structure, interaction between sulfur and carbon, and cell performance are researched. The Li−S battery furnished with the two carbon−sulfur hybrid materials as the cathode host material delivers a well reversible rate cycling performance, and a low decay rate of 0.037% and 0.056% per cycle during 1000 cycles at 1C for FLC and OLC, respectively, with a sulfur load of about 2.2 mg/cm^2. The excellent electrochemical performance of the two carbon materials obtained by detonation method makes them ideal substitute products of the commercial Super P carbon material, especially the FLC material.

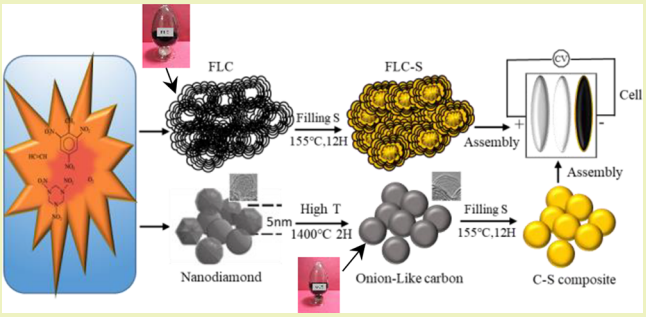

KEYWORDS: *Li−S batteries, Fullerene-shaped carbons, Hybrid cathodes, Detonation, Frameworks*

INTRODUCTION

Theoretical specific energy density of Li−S batteries can reach 2600 W h kg^{-1}, which is 5 times that of currently commercialized lithium-ion batteries and is regarded as the most promising next-generation lithium-ion battery.[1−4] However, Li−S batteries are limited by the poor conductivity of S and its end-product Li_2S,[5,6] the shuttle effect of intermediate product lithium polysulfide (LPS), and large volume expansion of active material during the charge−discharge process,[7−10] which cause the low S utilization, inferior rate performance, and poor cycling stability, and thus have been unable to meet the demands of commercial application.[3,11]

Carbon material additive in the active S cathode is a wise choice because of its excellent electrical conductivity, light weight, and low price.[12] Researchers try to shape the required morphology and add modifications of the carbon materials to retain their original electrical conductivity, while inhibiting the shuttle effect through encapsulating S and LPS within the carbon framework;[13−17] therefore, many sp^2 hybrid carbon materials emerge in various frameworks applied to Li−S batteries, such as carbon black,[18−20] super P,[21,22] mesoporous carbon,[23−25] carbon nanofiber,[26−28] carbon nanotube,[29−31] graphene nanosheet,[32,33] onion-like carbon (OLC),[34] and complex multichannel pore carbon material.[35,36] However, a detailed comparison of various conductive carbons on physical and electrochemical performance was short of reports in Li−S batteries, especially the carbon materials fabricated by gas detonation application for Li−S batteries, and have not been reported so far.

In this paper, two typical carbon materials synthesized by the detonation technique are selected as host for S cathode. The pore size distribution, pore volume, specific surface area, electronic conductivity, composite structure, interaction between sulfur and carbon, and cell performance are researched, which reminds us that carbon additive chosen is multifaceted trade-off; it provides a reference for the design and synthesis of carbon materials. Moreover, the detonation carbon material may replace the commercial carbon material application in Li−S battery.

EXPERIMENTAL SECTION

Commercial Super P carbon (SPC) as the control sample was purchased from Shenzhen Kejing Star Technology Co., Ltd. (Shenzhen, China). Fullerene-like carbon material (FLC) was from acetylene gas and a small amount of oxygen molecules through detonation technique and was executed by our cooperative enterprise

Received: April 8, 2019
Revised: June 14, 2019
Published: July 10, 2019

DOI: 10.1021/acssuschemeng.9b01951
ACS Sustainable Chem. Eng. 2019, 7, 12948−12954

Nafortis Technology Co., Ltd. (Shanghai, China). Onion-like carbon (OLC) was synthesized by thermal annealing nanodiamond carbon material, which was produced from TNT, RDX explosion, and purification by our cooperative company (Nafortis Technology Co., Ltd.), with a diameter in the range of 5−10 nm. The nanodiamond powders were annealed in a high vacuum of 10−2 Pa in a graphite crucible with a tungsten heater at 1400 °C for 2 h (heating/cooling rate: 10 °C min^{-1}) using a water-cooled high-temperature furnace to obtain OLC material.

Synthesis of C−S Composites. The C−S hybrid composite was prepared through a physical method of filling sulfur. After the investigation of the component ratios of carbon to sulfur, we noted that the morphology was more uniform with the ratios C:S = 3:7. So we mixed the 70 wt % S and 30 wt % carbon powders and ground them in a ball-milling machine to get nearly uniform distribution of the sulfur. Then the C−S composite powders were thermally annealed at 155 °C for 12 h in a crucible; the sulfur under this temperature is liquid with the minimum viscosity, and more likely to cover over all the available surface of the C particles.

Electrode Fabrication. The three different C−S composites powders were individually mixed with 8 wt % polyvinylidene fluoride (PVDF) binder in an *N*-methylpyrrolidinone (NMP) solution to attain the desired slurry viscosity. Then the slurry was spread onto a carbon paper current collector by a doctor blade and dried at 60 °C in vacuum for 12 h to get rid of any traces of solvent. The electrode was cut into disks with a diameter of 12 mm and the S loading on each disk is about 2.2 mg/cm^2. The 2032 coin cells were assembled in an Ar-filled glovebox, C−S composite disk as cathode materials, Li metal served as anode, and Celgard 2325 membrane used as separator; the electrolyte was composed of 1.0 M lithium bis-(trifluoromethanesulfonyl) imide (LiTFSI) and 5% $LiNO_3$ salts in a mixture of dimethoxymethane (DME) and 1,3-dioxolane (DOL) at a 1:1 volume ratio (Guo Tai Hua Rong Co.,Ltd.). The ratio of electrolyte and sulfur was about 20 μL/mg.

Characterization. Porosity analysis was carried out using an ASAP2020HD88 nitrogen gas sorption system (Micromeritics Instrument Corp, USA). The three kinds of carbon powders were initially outgassed at 100 °C for 1 h and then outgassed at 300 °C for 10 h under vacuum (100 μmHg). The nitrogen gas sorption analysis was performed at a temperature of −196 °C in the relative pressure range from 1×10^{-5} to 1.0. The pore size distribution was calculated using the density functional theory (DFT) methods. The BET surface area was calculated in the linear regime of the isotherms from 0.1 to 1.0 P/P_0. The structure of C was analyzed by the D8 Advance Diffractometer X-ray diffraction (Bruker, Germany) with a Cu Kα radiation. All samples were measured in a range from 10 to 60°. Renishaw inVia Reflex Raman Microscope was employed to record the Raman spectra with a laser operating at 532 nm. 1800 lines per mm grating and a 50× objective were used to reach a slit opening 65 μm. The laser spot on the sample was about 2 μm in diameter at a power of 0.1 mW. The acquisition time of each spectrum was 30 s, and 10 accumulations were averaged. Thermogravimetric analysis (TGA) was adopted using a PerkinElmer Diamond TG/DTA equipment. C−S composite was heated to 450 °C with a heating rate of 5 °C/min under continuous flow of nitrogen. So the loading of sulfur can be estimated under sulfur sublimes curves. XPS measurements were carried out on an Axis Ultra DLD X-ray photoelectron spectrometer using monochromatic Al Kα (1486.6 eV) radiation. SEM characterization was conducted using Hitachi S4800 (Japan); TEM were characterized by FEI Tecnai F20 field emission scanning transmission electron microscope at 300 keV.

Electrochemical Test. Long cycling stability, rate capacity, and discharge/charge performances were evaluated through a Neware Battery Measurement System in the voltage range of 3.0−1.8 V (vs Li^+/Li). The electrochemical impedance spectroscopy (EIS) of the cells was recorded with a CHI660E electrochemical workstation (Shanghai ChenHua Co., Ltd.) over the frequency range of 100 kHz to 100 mHz.

RESULTS AND DISCUSSION

The SPC, FLC, and OLC powders are basically spherical with a mean size of 50, 40, and 5 nm, respectively (Figure 1). (i)

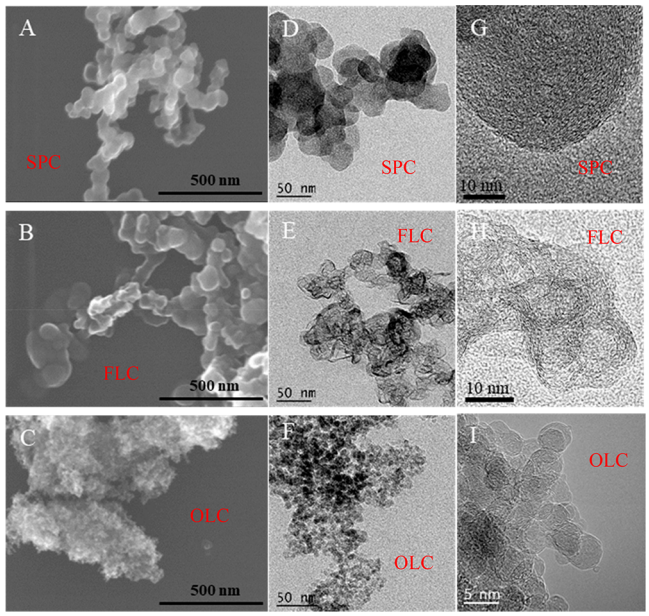

Figure 1. (A−C) SEM and (D−I) TEM images of these carbon materials.

The SPC sample has a closed spheroid-like graphite morphology, solid sphere structure. (ii) For the FLC, the outside shell is stacked with multilayer graphene of about 6−13 layers, the hollow inside shell is obviously present with the diameter range of 3−8 nm, the shell surface is clearly bent and out of shape, and the shell thickness is approximately 4−8 nm; the internal hollow shell structure helps to reserve space for the volume expansion of the active material, and the outer graphene sheet structure can provide good conductivity in the discharge and charge process. (iii) For the OLC, it is a spherical particle with a stacked graphene of less than 10 layers; there may be untransformed nanodiamond structures in the center. The small size sphere provides large specific surface area, which is a benefit for loading more active material, while the graphene with excellent conductivity is beneficial for the rate performance of the Li−S batteries.[37]

From the XRD test (Figure 2), the diffraction peak at 44° corresponds to the (111) of the diamond, combined with TEM micrograph, which means the OLC contains untransformed nanodiamond phase in the center of the fullerene ball. The peak at about 26° is corresponding to the (002) plane of graphite materials, showing good electrical conductivity of the three carbon materials. The main peak of SPC shifts a little to the small angle, presenting some amorphous carbon in it. For FLC, the peak at about 19° indicates the parts of graphite oxide inside; this was confirmed in the XPS (Figure S2) test. The peaks observed in the XPS pattern demonstrate the presence of C 1s and O 1s on the surface of FLC. The C 1s spectra contains four peaks, representing C−C/C═C, C−O, C═O, and O−C═O, respectively. The oxygen atoms mainly exist in forms of C═O and C−O. The oxygen atomic concentrations in the FLC material are considerable. The polar-philic oxygen-containing functional groups have been proven as active reaction sites showing strong chemical binding

DOI: 10.1021/acssuschemeng.9b01951
ACS Sustainable Chem. Eng. 2019, 7, 12948−12954

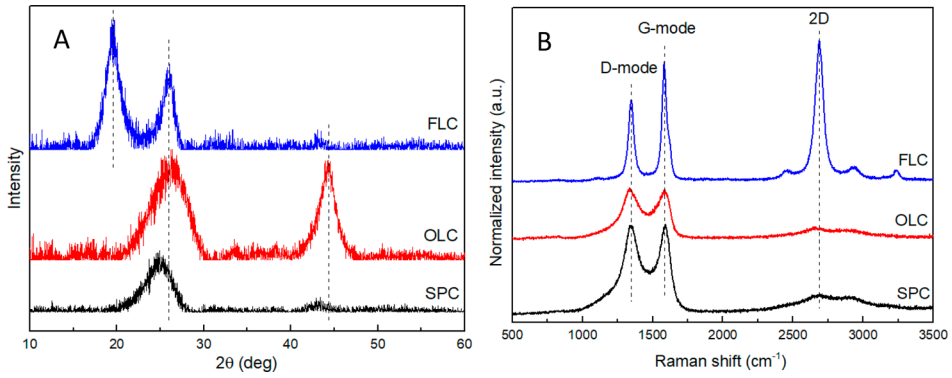

Figure 2. (A) XRD curves and (B) Raman spectra of the three carbon materials.

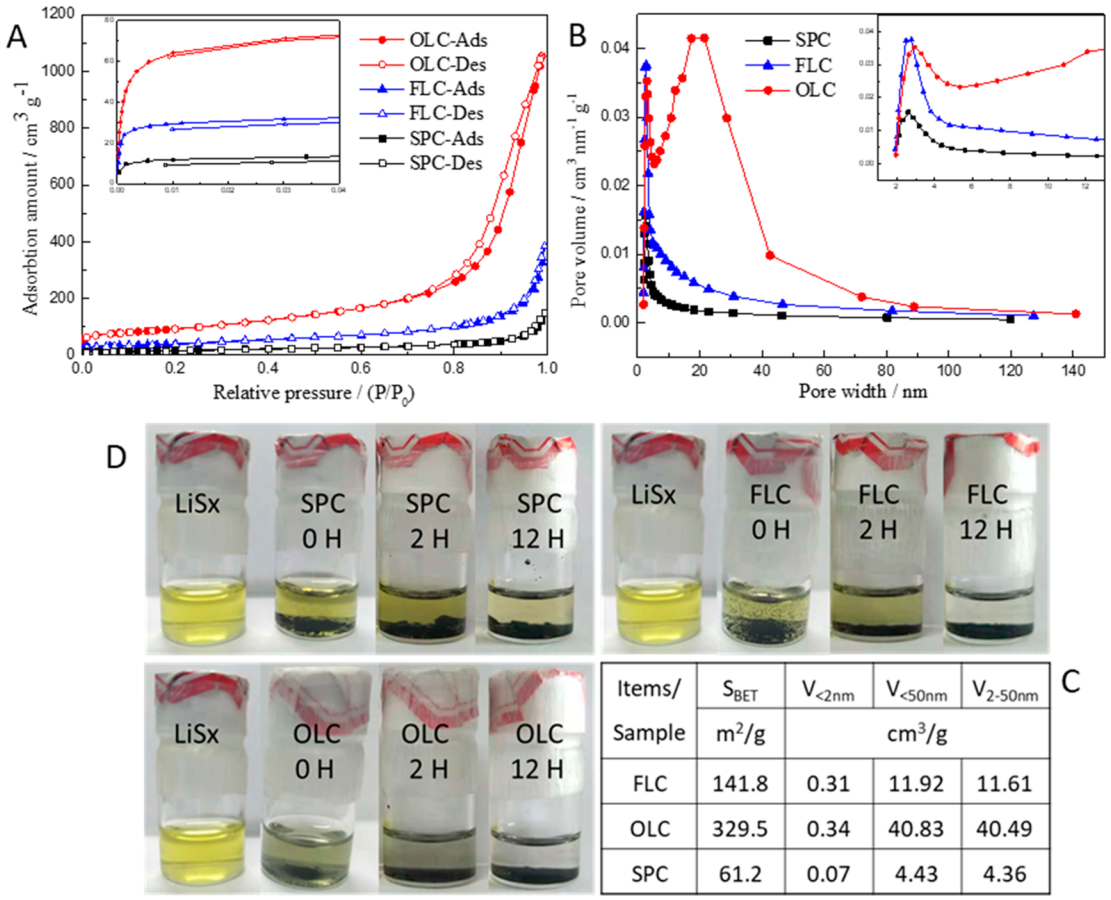

C

Items/ Sample	S_{BET}	$V_{<2nm}$	$V_{<50nm}$	$V_{2\text{-}50nm}$
	m^2/g	cm^3/g		
FLC	141.8	0.31	11.92	11.61
OLC	329.5	0.34	40.83	40.49
SPC	61.2	0.07	4.43	4.36

Figure 3. (A) Nitrogen adsorption−desorption isotherms of carbon materials, (B) pore width distribution, (C) table of pore size distribution, and (D) visualization photos of LPS adsorption.

capabilities with LPS,[38−40] which is in agreement with the adsorption experiment's results in Figure 3D.

Three different types of carbon materials are characterized by their typical Raman spectrum with the carbon D-mode at 1340 cm^{-1}, the G-mode at 1584 cm^{-1}, and a distinct second-order spectrum. The G-mode, representative of sp^2-hybridized carbon, indicates nanocrystalline and partially amorphous carbon. The D-mode is caused by the disorder and defects in carbon materials; the fact that the three carbon materials all contain D-mode confirms the lattice defects inside. In general, the graphitization degree of carbon materials is evaluated by the intensity ratio between G peak and D peak; for OLC, FLC, and SPC, the value of I_G/I_D is about 0.97, 1.46, and 1.01, respectively, indicating the FLC material present at a rather high degree of ordering as demonstrated by the sharp G-mode. The distinct second-order peak at 2685 cm^{-1} represents the vibration mode of two photonic lattices, which is the frequency doubling peak of D peak. Generally, the I_{2D}/I_G value of high-quality (no defects) monolayer graphene is 2. And the graphene layers are getting thicker with the reduction of the proportion. Compared to OLC and SPC, FLC has thinner graphene layers. Perhaps the graphene layer is tightly stacked for OLC and SPC material, causing their unconspicuous 2D peak.

The characteristics of the three kinds of carbon materials of the nitrogen adsorption−desorption curves are presented in

DOI: 10.1021/acssuschemeng.9b01951
ACS Sustainable Chem. Eng. 2019, 7, 12948−12954

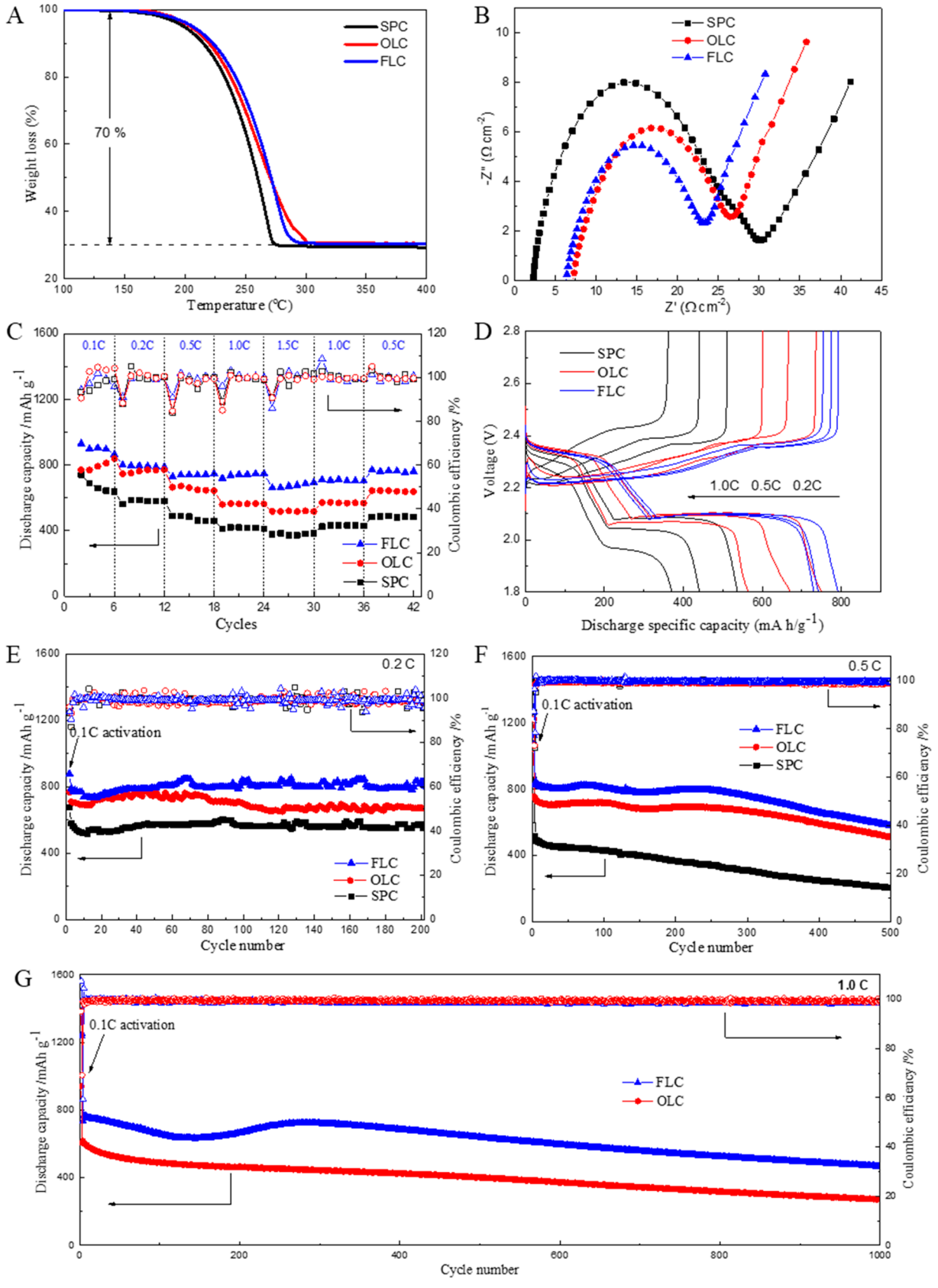

Figure 4. (A) Sulfur content measurement curves of TGA. (B) Electrochemical impedance spectroscopy patterns of the three carbon materials. (C) Rate performances of the three carbon materials. (D) Charge/discharge profiles in rate test. Cycling capacity and Coulombic efficiency of carbon materials at (E) 0.2C, (F) 0.5C, and (G) 1.0C.

DOI: 10.1021/acssuschemeng.9b01951
ACS Sustainable Chem. Eng. 2019, 7, 12948−12954

Figure 3A,B. According to the isotherm linear plot (Figure 3A, insert curve), at a very low relative pressure P/P_0 between 0 and 0.005, there exists a sharp adsorption feature in the curves, especially for OLC and FLC, indicating the micropores (<2 nm) in these materials. A large number of micropores can play a certain physical adsorption on the polysulfide produced during charging and discharging process and improve the circulation stability of the Li−S batteries. The desorption branch of OLC illustrates a large hysteresis loop in the range of P/P_0 = 0.7−1 with a closure P/P_0 of about 0.7, representing capillary adsorption exists in this material and OLC material contains rich mesopores (2−50 nm), which is strongly proven in Figure 3B, a strong peak in the range 5−50 nm. Generally, mesopores are good places to store the active material sulfur through the physical filling S element; moreover, they can also provide a good buffer space for the volume change of active substances. However, for the FLC and SPC material, the lag ring is not obvious, indicating they have a few mesopores.[41] In the range of 2−4 nm pore size, FLC has equivalent pore volume with OLC; it is confirmed to have excellent confinement ability for sulfur. According to Figure 3C, the BET specific surface area of FLC, OLC, and SPC materials are 141.8, 329.5, and 61.2 m^2/g and pore volume (V < 50 nm) of 11.92, 40.83, and 4.43 cm^3/g, respectively. The micropores and mesopores volumes of SPC material is only 0.07 and 4.36 cm^3/g, a negligible amount. The differentiated pores are formed through different routes, on the particles surface, interior of particles, or between particles agglomerates; some slits are formed by the accumulation of particles. These pores or slits among the particle interstices were utilized to embed insulating sulfur to attain a high degree of intimate contact with the carbon surfaces; moreover, the hierarchy pores also play a crucial role in the functioning of Li−S batteries by accommodating a large quantity of S mass as well as electrolyte wetting together with lowering the tendency of polysulfide migration out of the cathode to the bulk electrolyte. According to the visualization photos of LPS adsorption (Figure 3 D), abundant pore structure of OLC obviously can adsorb solved LPS, while FLC can also achieve a significant adsorption effect after a long period of time for adsorption; however, commercial SPC has almost no adsorption for LPS and cannot inhibit the shuttle effect. FLC contains equivalent micropores and fewer mesopores than OLC, in the experiment of adsorbing LPS; it can be concluded that the mesoporous adsorption LPS plays a dominant role.

After the investigation of the component ratios of carbon to sulfur, we note that the morphology is more uniform with the ratios C:S = 3:7 (Figure S1). So we choose this proportion for electrochemical evaluation. Thermogravimetric analysis of FLC-S, OLC-S, and SPC-S compounds shows very little mass loss of ca. 1% to 450 °C; heating rate is 5 °C/min. The mass loss is attributed to the decomposition of active material S. From the TGA curves (Figure 4A), at low temperature, the order of desulfurization is SPC, OLC, and FLC, respectively. Since the rich mesopores of OLC are interstitial spaces of particles, sulfur is outside the particle and is encased to the bared surface of the OLC, making it easier to escape. For FLC, the pores may be in the center of the particle, parts of sulfur may penetrate the interior of the particles, there are graphene shells outside, and the desulfurization temperature should be the highest. However, in the high-temperature range, the FLC will be desulfurized before OLC because the rich micropores and mesopores of OLC can physically adsorb the sulfur, and need a high temperature to disengage in the case where the sulfur is almost exhausted. The adsorption of micropores and mesoporous is dominant, obviously; OLC is the last to remove sulfur, at high temperature. This characteristic is consistent with previous BET test results.

The electrochemical impedance spectroscopy (EIS) of the fresh cells is exhibited in Figure 4B; all the greatly suppressed semicircle diameters at low frequency explain the decreased charge-transfer resistances. And almost the same ohm impedance values of those materials indicate the explored carbon material FLC and OLC will not trigger obvious changes in ohm resistance of the cell. The EIS data are in agreement with the following cycling performances at 0.2C and 0.5C.

The discharge specific capacities and Coulombic efficiencies are acquired under different current rates (Figure 4C) at 0.1, 0.2, 0.5, 1.0, and 1.5C, respectively, under the sulfur loading of about 2.2 mg cm^{-2}. The high discharge capacity of 0.1C demonstrates the enhanced active material utilization of the FLC material; moreover, the specific capacities of 711 and 770 mA h g^{-1} are recovered when the current density switches back to 1.0 and 0.5 C, near or even beyond the amount before the current switching, suggesting well reversible rate cycling performance. For the OLC material and SPC, they also have good rate recovery performance. Although OLC has a larger surface area, the discharge capacity is not good enough; the active material is basically exposed to the surface of the material, not conducive to the active material volume scaling and not beneficial to utilization of active substances in the discharge process; and it is obvious in the case of large rate discharge in the following test at 1.0C. The hollow internal structure of the FLC gives good storage space for sulfur; even in the process of changing the volume, it has a good performance.

Charge/discharge voltage profiles of the three carbon materials exhibit two discharge plateaus that are consistent with the cyclic voltammogram plots (Figure 4D). The upper discharge plateau indicates the transformation of elemental sulfur to soluble long-chain LPS ions S_{n-2} ($4 < n < 8$), and the lower discharge plateau suggests the transformation of long-chain LPS to short-chain LPS, Li_2S_2, and Li_2S, which are also the inherent discharge platform curve of lithium−sulfur batteries.[5] The change of carbon material structure will not cause the great change of Li−S discharge platform; the phenomenon of the last tail of OLC discharge platform is generally believed to be caused by obvious micro-mesoporous materials,[42−44] and therefore, increasing the material micro-mesoporous can improve the discharge specific capacity of the battery in the low voltage area.

For the three carbon materials examined at 0.2C (Figure 4E), an initial capacity of 792, 723, and 676 mA h g^{-1} of FLC, OLC, and SPC, respectively, and a retained capacity of 721, 626, and 559 mA h g^{-1} after 200 cycles are obtained, corresponding to the capacity retention of 91%, 87%, and 83%, respectively. However, for the 0.5C (Figure 4F), the capacity retention of the FLC, OLC, and SPC stays at 54%, 67%, and 25% after 500 charge and discharge cycles, respectively; the FLC materials have the highest initial capacity of 792 mA h g^{-1}. The properties of carbon materials obtained by detonation method are obviously better than the commercial SPC material and can be a substitute product.

The long-term cycling of FLC and OLC is performed at 1.0C rate (Figure 4G). After activation at 0.1C, an initial capacity of 734 and 616 mA h g^{-1} is obtained. And it delivers a

DOI: 10.1021/acssuschemeng.9b01951
ACS Sustainable Chem. Eng. 2019, 7, 12948−12954

low decay rate of 0.037% and 0.056% per cycle during 1000 cycles at 1C for FLC and OLC respectively. The satisfactory cycling performance is primarily attributed to the favorable micropores, mesopores, and internal structure of FLC and OLC. The thin carbon shell of FLC with limited micropores volume immobilizes the long-chain LPS, meanwhile enabling unhindered access of Li^+ with smaller particle size. From the XRD spectrum, some active sites may be on the surface of the FLC that may chemically anchor the dissolved LPS. Furthermore, the different pores provide fairly active contact surface, enabling quick electron transfer for the follow-up redox reaction, which speeds up the transformation of LPS from ionic state to the insoluble end product.

CONCLUSIONS

Our work researched OLC and FLC fabricated from gas detonation method for C/S hybrid cathodes for lithium−sulfur batteries with sulfur loading up to 70 mass % and without any further addition of a conducting aid such as carbon black or SPC. We explored ball milling and physical filling sulfur. The electrochemical performance of three hybrid materials was tested by electrochemical characterization. FLC and OLC boasted an optimum interaction between the hybrid components exhibiting a specific capacity of 721 mA h g^{-1} even after 200 charge−discharge cycles at specific current 0.2C discharge rate. In addition, the capacity restoration ability of FLC after running with a high current density of 1675 mA g^{-1} (corresponds to 1.0 C discharge rate) showed a specific capacity of 734 mA h g^{-1} close to its earlier capacity at 0.2C rate (792 mA h g^{-1}). This hybrid material demonstrated an enhanced performance compared to the commercial SPC hybrids. Among them, the hybrid cathode material of FLC was superior since the sulfur nanoparticles could be found inside the hollow center of the FLC through thermal annealing.

However, OLC provides an exclusively outer surface, enabling the synergy of high sulfur mass loading and a high percentage of electrochemically active sulfur. The sulfur on the surface is however easily lost and dissolved in the electrolyte. This leads to rapid decay in cell performance and makes it necessary to build a house to store the active material without affecting the ions transmission. Moreover, micro- and mesopores on the surface are necessary. Therefore, the pursuit of specific surface area cannot solely solve the existing problems in Li−S batteries; we need to involve the design of carbon pores distribution and good space structure to limit the shuttle effect of lithium polysulfide. This provides ideas for us to reoptimize the structure in the next step. Obviously, in the 0.5 and 1.0C cycles, the battery capacity attenuation accelerates after 250 cycles; therefore, the medium- and long-term cyclic stability is also the key we need to carefully study and solve further.

ASSOCIATED CONTENT

Supporting Information

The Supporting Information is available free of charge on the ACS Publications website at DOI: 10.1021/acssuschemeng.9b01951.

SEM of FLC at different sulfur filling ratios and magnification ratios; XPS of FLC carbon material (PDF)

AUTHOR INFORMATION

Corresponding Authors

*E-mail: xhfeng@nimte.ac.cn (X.H.F.).
*E-mail: yangzhou.ma@outlook.com (Y.Z.M.).
*E-mail: lihua@nimte.ac.cn (H.L.).

ORCID

Xiaohua Feng: 0000-0001-5931-9321
Hua Li: 0000-0002-8786-4295

Notes

The authors declare no competing financial interest.

ACKNOWLEDGMENTS

This project is supported by National Natural Science Foundation of China through Grant No. 51802322, Ningbo Natural Science Foundation Grant No. 2018A610082, and S&T Innovation 2025 Major Special Programme of Ningbo (2018B10054). One of the authors, Yangzhou Ma, is grateful for Anhui Natural Science Foundation No.1908085ME151.

REFERENCES

(1) Wang, J. L.; Yang, J.; Wan, C. R.; Du, K.; Xie, J. Y.; Xu, N. X. Sulfur composite cathode materials for rechargeable lithium batteries. *Adv. Funct. Mater.* **2003**, *13*, 487−492.

(2) Xiao, L. F.; Cao, Y. L.; Xiao, J.; Schwenzer, B.; Engelhard, M. H.; Saraf, L. V.; Nie, Z.; Exarhos, G. J.; Liu, J. A Soft Approach to Encapsulate Sulfur: Polyaniline Nanotubes for Lithium-Sulfur Batteries with Long Cycle Life. *Adv. Mater.* **2012**, *24*, 1176−1181.

(3) Song, M. K.; Cairns, E. J.; Zhang, Y. G. Lithium/sulfur batteries with high specific energy: old challenges and new opportunities. *Nanoscale* **2013**, *5*, 2186−2204.

(4) Yin, Y. X.; Xin, S.; Guo, Y. G.; Wan, L. J. Lithium-Sulfur Batteries: Electrochemistry, Materials, and Prospects. *Angew. Chem., Int. Ed.* **2013**, *52*, 13186−13200.

(5) Kang, W. M.; Deng, N. P.; Ju, J. G.; Li, Q. X.; Wu, D. Y.; Ma, X. M.; Li, L.; Naebe, M.; Cheng, B. A review of recent developments in rechargeable lithium-sulfur batteries. *Nanoscale* **2016**, *8*, 16541−16588.

(6) Cheon, S. E.; Ko, K. S.; Cho, J. H.; Kim, S. W.; Chin, E. Y.; Kim, H. T. Rechargeable lithium sulfur battery - I. Structural change of sulfur cathode during discharge and charge. *J. Electrochem. Soc.* **2003**, *150*, A796−A799.

(7) Zheng, D.; Liu, D.; Harris, J. B.; Ding, T. Y.; Si, J. Y.; Andrew, S.; Qu, D. Y.; Yang, X. Q.; Qu, D. Y. Investigation of the Li-S Battery Mechanism by Real-Time Monitoring of the Changes of Sulfur and Polysulfide Species during the Discharge and Charge. *ACS Appl. Mater. Interfaces* **2017**, *9*, 4326−4332.

(8) Ji, X. L.; Lee, K. T.; Nazar, L. F. A highly ordered nanostructured carbon-sulphur cathode for lithium-sulphur batteries. *Nat. Mater.* **2009**, *8*, 500−506.

(9) Wu, Y. L.; Yang, J.; Wang, J. L.; Yin, L. C.; Nuli, Y. N. Composite Cathode Structure and Binder for High Performance Lithium-Sulfur Battery. *Acta Phys.-Chim. Sin.* **2010**, *26*, 283−290.

(10) Wang, C.; Chen, J. J.; Shi, Y. N.; Zheng, M. S.; Dong, Q. F. Preparation and performance of a core-shell carbon/sulfur material for lithium/sulfur battery. *Electrochim. Acta* **2010**, *55*, 7010−7015.

(11) Liang, X.; Wen, Z. Y.; Liu, Y. New Development of Key Materials for High-Performance Lithium-Sulfur Batteries. *Prog. Chem.-Beijing* **2011**, *23*, 520−526.

(12) Yuan, L. X.; Yuan, H. P.; Qiu, X. P.; Chen, L. Q.; Zhu, W. T. Improvement of cycle property of sulfur-coated multi-walled carbon nanotubes composite cathode for lithium/sulfur batteries. *J. Power Sources* **2009**, *189*, 1141−1146.

(13) Peng, H. J.; Huang, J. Q.; Zhao, M. Q.; Zhang, Q.; Cheng, X. B.; Liu, X. Y.; Qian, W. Z.; Wei, F. Nanoarchitectured Graphene/CNT@Porous Carbon with Extraordinary Electrical Conductivity and

DOI: 10.1021/acssuschemeng.9b01951
ACS Sustainable Chem. Eng. 2019, 7, 12948−12954

Interconnected Micro/Mesopores for Lithium- Sulfur Batteries. *Adv. Funct. Mater.* **2014**, *24*, 2772−2781.
(14) Xu, G. Y.; Ding, B.; Nie, P.; Shen, L. F.; Dou, H.; Zhang, X. G. Hierarchically Porous Carbon Encapsulating Sulfur as a Superior Cathode Material for High Performance Lithium-Sulfur Batteries. *ACS Appl. Mater. Interfaces* **2014**, *6*, 194−199.
(15) Zhou, G. M.; Pei, S. F.; Li, L.; Wang, D. W.; Wang, S. G.; Huang, K.; Yin, L. C.; Li, F.; Cheng, H. M. A Graphene-Pure-Sulfur Sandwich Structure for Ultrafast, Long-Life Lithium-Sulfur Batteries. *Adv. Mater.* **2014**, *26*, 625−631.
(16) Zhang, Z. W.; Li, Z. Q.; Hao, F. B.; Wang, X. K.; Li, Q.; Qi, Y. X.; Fan, R. H.; Yin, L. W. 3D Interconnected Porous Carbon Aerogels as Sulfur Immobilizers for Sulfur Impregnation for Lithium-Sulfur Batteries with High Rate Capability and Cycling Stability. *Adv. Funct. Mater.* **2014**, *24*, 2500−2509.
(17) Sun, Q.; He, B.; Zhang, X. Q.; Lu, A. H. Engineering of Hollow Core-Shell Interlinked Carbon Spheres for Highly Stable Lithium-Sulfur Batteries. *ACS Nano* **2015**, *9*, 8504−8513.
(18) Jeon, B. H.; Yeon, J. H.; Kim, K. M.; Chung, I. J. Preparation and electrochemical properties of lithium-sulfur polymer batteries. *J. Power Sources* **2002**, *109*, 89−97.
(19) Li, G. C.; Li, G. R.; Ye, S. H.; Gao, X. P. A Polyaniline-Coated Sulfur/Carbon Composite with an Enhanced High-Rate Capability as a Cathode Material for Lithium/Sulfur Batteries. *Adv. Energy Mater.* **2012**, *2*, 1238−1245.
(20) Li, G. C.; Hu, J. J.; Li, G. R.; Ye, S. H.; Gao, X. P. Sulfur/activated-conductive carbon black composites as cathode materials for lithium/sulfur battery. *J. Power Sources* **2013**, *240*, 598−605.
(21) Hao, Z. X.; Yuan, L. X.; Li, Z.; Liu, J.; Xiang, J. W.; Wu, C.; Zeng, R.; Huang, Y. H. High performance lithium-sulfur batteries with a facile and effective dual functional separator. *Electrochim. Acta* **2016**, *200*, 197−203.
(22) Li, T.; Bo, H.; Cao, H. W.; Lai, Y. Q.; Liu, Y. X.; Huang, Z. X. Effects of Carbon Hosts on Electrochemical Properties of Lithium-Sulfur Batteries. *Int. J. Electrochem. Sci.* **2017**, *12*, 5731−5741.
(23) Sun, Z. J.; Wang, S. J.; Yan, L. L.; Xiao, M.; Han, D. M.; Meng, Y. Z. Mesoporous carbon materials prepared from litchi shell as sulfur encapsulator for lithium-sulfur battery application. *J. Power Sources* **2016**, *324*, 547−555.
(24) Mi, K.; Jiang, Y.; Feng, J. K.; Qian, Y. T.; Xiong, S. L. Hierarchical Carbon Nanotubes with a Thick Microporous Wall and Inner Channel as Efficient Scaffolds for Lithium-Sulfur Batteries. *Adv. Funct. Mater.* **2016**, *26*, 1571−1579.
(25) Nitze, F.; Fossum, K.; Xiong, S. Z.; Matic, A.; Palmqvist, A. E. C. Sulfur-doped ordered mesoporous carbons: A stability-improving sulfur host for lithium-sulfur battery cathodes. *J. Power Sources* **2016**, *317*, 112−119.
(26) Fang, X.; Weng, W.; Ren, J.; Peng, H. S. A Cable-Shaped Lithium Sulfur Battery. *Adv. Mater.* **2016**, *28*, 491−496.
(27) Choi, S. H.; Song, J. J.; Wang, C. Y.; Park, S.; Wang, G. X. Multifunctional Free-Standing Gel Polymer Electrolyte with Carbon Nanofiber Interlayers for High-Performance Lithium-Sulfur Batteries. *Chem. - Asian J.* **2017**, *12*, 1470−1474.
(28) Yuan, Y.; Fang, Z.; Liu, M. B. Sulfur/hollow Carbon Nanofiber Composite as Cathode Material for Lithium-Sulfur Batteries. *Int. J. Electrochem. Sci.* **2017**, *12*, 1025−1033.
(29) Liu, X. Y.; Huang, W. L.; Wang, D. D.; Tian, J. H.; Shan, Z. Q. A nitrogen-doped 3D hierarchical carbon/sulfur composite for advanced lithium sulfur batteries. *J. Power Sources* **2017**, *355*, 211−218.
(30) Sun, L.; Li, M. Y.; Jiang, Y.; Kong, W. B.; Jiang, K. L.; Wang, J. P.; Fan, S. S. Sulfur Nanocrystals Confined in Carbon Nanotube Network As a Binder-Free Electrode for High-Performance Lithium Sulfur Batteries. *Nano Lett.* **2014**, *14*, 4044−4049.
(31) Zhang, Q.; Cheng, X. B.; Huang, J. Q.; Peng, H. J.; Wei, F. Review of carbon materials for advanced lithium-sulfur batteries. *New Carbon Materials* **2015**, *81*, 850.
(32) Hao, Y.; Li, X. F.; Sun, X. L.; Wang, C. L. Nitrogen-doped graphene nanosheets/sulfur composite as lithium-sulfur batteries cathode. *Mater. Sci. Eng., B* **2016**, *213*, 83−89.
(33) Zhang, Z.; Kong, L. L.; Liu, S.; Li, G. R.; Gao, X. P. A High-Efficiency Sulfur/Carbon Composite Based on 3D Graphene Nanosheet@Carbon Nanotube Matrix as Cathode for Lithium-Sulfur Battery. *Adv. Energy Mater.* **2017**, *7*, 1602543.
(34) Choudhury, S.; Zeiger, M.; Massuti-Ballester, P.; Fleischmann, S.; Formanek, P.; Borchardt, L.; Presser, V. Carbon onion-sulfur hybrid cathodes for lithium-sulfur batteries. *Sustainable Energy & Fuels* **2017**, *1*, 84−94.
(35) Wang, Q.; Yang, M. H.; Wang, Z. B.; Li, C.; Gu, D. M. Functional Differentiation of Three Pores for Effective Sulfur Confinement in Li-S Battery. *Small.* **2018**, *14*, 1703279.
(36) Wang, Q.; Wang, Z. B.; Yang, M. H.; Li, C.; Gu, D. M. A novel synthetic route to cathode materials for Li-S batteries: from organic sulfides to sulfur/nitrogenous carbon composites. *J. Mater. Chem. A* **2017**, *5*, 16796−16802.
(37) Li, C.; Sui, X. L.; Wang, Z. B.; Wang, Q.; Gu, D. M. 3D N-doped graphene nanomesh foam for long cycle life lithium-sulfur battery. *Chem. Eng. J.* **2017**, *326*, 265−272.
(38) Mi, K.; Chen, S. W.; Xi, B. J.; Kai, S. S.; Jiang, Y.; Feng, J. K.; Qian, Y. T.; Xiong, S. L. Sole Chemical Confinement of Polysulfides on Nonporous Nitrogen/Oxygen Dual-Doped Carbon at the Kilogram Scale for Lithium-Sulfur Batteries. *Adv. Funct. Mater.* **2017**, *27*, 1604265.
(39) Liu, J. H.; Li, W. F.; Duan, L. M.; Li, X.; Geng, Z. B.; Huang, K. K.; Lu, L. H.; Zhou, L. S.; Liu, Z. R.; Chen, W.; Liu, L. W.; Feng, S. H.; Zhang, Y. G.; Ji, L. A Graphene-like Oxygenated Carbon Nitride Material for Improved Cycle-Life Lithium/Sulfur Batteries. *Nano Lett.* **2015**, *15*, 5137−5142.
(40) Yu, M. P.; Ma, J. S.; Song, H. Q.; Wang, A.; Tian, F. Y.; Wang, Y. S.; Qiu, H.; Wang, R. M. Atomic layer deposited TiO2 on a nitrogen-doped graphene/sulfur electrode for high performance lithium-sulfur batteries. *Energy Environ. Sci.* **2016**, *9*, 1495−1503.
(41) Li, C.; Sui, X. L.; Wang, Z. B.; Wang, Q.; Gu, D. M. One-step synthesis of 3D N-doped graphene supported metal oxide for high performance Li-S battery. *Ceram. Int.* **2018**, *44*, 13419−13425.
(42) Lyu, Z. Y.; Xu, D.; Yang, L. J.; Che, R. C.; Feng, R.; Zhao, J.; Li, Y.; Wu, Q.; Wang, X. Z.; Hu, Z. Hierarchical carbon nanocages confining high-loading sulfur for high-rate lithium-sulfur batteries. *Nano Energy* **2015**, *12*, 657−665.
(43) Zheng, J. H.; Guo, G. N.; Li, H. W.; Wang, L.; Wang, B. W.; Yu, H. J.; Yan, Y. C.; Yang, D.; Dong, A. G. Elaborately Designed Micro-Mesoporous Graphitic Carbon Spheres as Efficient Polysulfide Reservoir for Lithium-Sulfur Batteries. *Acs Energy Letters* **2017**, *2*, 1105−1114.
(44) Li, M.; Zhang, Y. N.; Wang, X. L.; Ahn, W.; Jiang, G. P.; Feng, K.; Lui, G.; Chen, Z. W. Gas Pickering Emulsion Templated Hollow Carbon for High Rate Performance Lithium Sulfur Batteries. *Adv. Funct. Mater.* **2016**, *26*, 8408−8417.

DOI: 10.1021/acssuschemeng.9b01951
ACS Sustainable Chem. Eng. 2019, 7, 12948−12954